Bioactive Materials 8 (2022) 559–572

Contents lists available at ScienceDirect

Bioactive Materials

journal homepage: www.sciencedirect.com/journal/bioactive-materials

A baicalin-loaded coaxial nanofiber scaffold regulated inflammation and osteoclast differentiation for vascularized bone regeneration

Shue Jin [a], Jing Gao [a], Renli Yang [b], Chen Yuan [a], Ruili Wang [c], Qin Zou [a], Yi Zuo [a], Meifang Zhu [c], Yubao Li [a], Yi Man [b], Jidong Li [a,*]

[a] Research Center for Nano-Biomaterials, Analytical and Testing Center, Sichuan University, Chengdu, 610064, PR China
[b] State Key Laboratory of Oral Diseases, West China Hospital of Stomatology, Sichuan University, Chengdu, 610065, PR China
[c] State Key Laboratory for Modification of Chemical Fibers and Polymer Materials, College of Materials Science and Engineering, Donghua University, Shanghai, 201620, PR China

ARTICLE INFO

Keywords:
Coaxial nanofiber
Baicalin
Inflammation
Osteoclast differentiation
Vascularized bone regeneration

ABSTRACT

We demonstrate a simple, effective and feasible method to address the shrinkage of Poly (lactic-*co*-glycolic acid) (PLGA) through a core-shell structure fiber strategy. The results revealed that introducing size-stable poly-caprolactone (PCL) as the core fiber significantly improved the PLGA-based fibrous scaffold's dimensional maintenance. We further utilized fish collagen to modify the PLGA shell layer (PFC) of coaxial fibers and loaded baicalin (BA) into the PCL core layer (PCL-BA) to endow fibrous scaffold with more functional biological cues. The PFC/PCL-BA fibrous scaffold promoted the osteogenic differentiation of bone mesenchymal stem cells and stimulated the RAW264.7 cells to polarize into a pro-reparative phenotype. Importantly, the *in vivo* study demonstrated that the PFC/PCL-BA scaffold could regulate inflammation and osteoclast differentiation, favor neovascularization and bone formation. This work tactfully combined PLGA and PCL to establish a drug release platform based on the core-shell fibrous scaffold for vascularized bone regeneration.

1. Introduction

Bone tissue regeneration is a complex interdisciplinary course of biomedical science and materials science, in which the regulation of the immune microenvironment, the dynamic balance between bone formation and bone resorption, and the construction of neovascularization network are extremely important [1,2]. Active regulation of the immune microenvironment in the early stage of implantation and subsequent vascular network formation is considered a prerequisite for successful functional bone regeneration because it was essential for cell recruitment, cytokine secretion and the transportation of oxygen, nutrients and metabolic waste [3–5]. Despite the fact that various bone regeneration scaffolds have been developed, researchers have never stopped exploring the construction of a scaffold that can genuinely realize vascularized bone regeneration [6]. In this work, we are committed to preparing a bone graft substitute with an extracellular matrix (ECM) like structure that can actively regulate the immune microenvironment and promote vascularized bone regeneration.

Poly (lactic-*co*-glycolic acid) (PLGA) and poly-caprolactone (PCL) are commonly used biomedical polymers; they have already been approved by the Food and Drug Administration (FDA) as a constituent of many biopolymer-based devices and has been widely used in the fields of nerve, skin, muscle and bone tissue engineering due to its good biocompatibility [7–11]. However, a severe defect of PLGA itself does not seem to attract enough attention, that is, dimensional instability [12]. PLGA quickly shrinks and deforms when stimulated by physical or chemical factors such as ultraviolet irradiation, liquid medium immersion, thermal treatment and ethylene oxide atmosphere [13–16]. PCL, a semi-crystalline polymer, was not easy to shrink or was even slightly swelling, but the implantation of unmodified PCL *in vivo* could easily cause excessive inflammation [17–19]. These weaknesses of PLGA and PCL limited its broader application in tissue engineering. With these in mind, we intend to utilize the coaxial fiber strategy as a simple, practical and feasible method to solve electrospun PLGA fibrous scaffold shrinkage and the relatively weak wettability of PCL. The inner PCL can inhibit the shrinkage of PLGA, and the outer PLGA can also seclude the

Peer review under responsibility of KeAi Communications Co., Ltd.
* Corresponding author.
E-mail address: nic1979@scu.edu.cn (J. Li).

https://doi.org/10.1016/j.bioactmat.2021.06.028
Received 11 April 2021; Received in revised form 1 June 2021; Accepted 23 June 2021
Available online 30 June 2021
2452-199X/© 2021 The Authors. Publishing services by Elsevier B.V. on behalf of KeAi Communications Co. Ltd. This is an open access article under the CC BY-NC-ND license (http://creativecommons.org/licenses/by-nc-nd/4.0/).

weak wettability caused by PCL. Evidently, this design could maximize the advantages of PLGA and PCL, and remedy for respective disadvantages.

Subsequently, we modified the coaxial fiber scaffold to confer good biological activity and make the scaffold more suitable for bone regeneration. Based on our previous study, we planned to introduce fish collagen (FC) into the shell of the coaxial fiber to improve biocompatibility and accelerate the degradation rate of the whole scaffold [20]. Another critical factor that should be considered is that the fibrous scaffold's efficiency without bioactive factors was limited for promoting bone regeneration [21]. The incorporation of growth factors such as bone morphogenetic protein 2 (BMP-2) and insulin-like growth factor 2 (IGF2) into biomaterials could effectively promote bone tissue regeneration [22]. However, there is a problem of inactivation in the loading of these biological factors into scaffolds [23–25]. Therefore, we designed our scaffold to load a more stable Chinese herbal component, baicalin (BA), into the core layer of the coaxial fiber instead of growth factors to enhance the bioactivity of the scaffold. BA, a flavonoid compound, has numerous merits, including anti-inflammatory and antibacterial properties, promotion of osteogenic differentiation and inhibition of osteoclastic differentiation, which works in a dose-dependent manner [26–29]. In this study, we attempted to introduce BA into electrospun fibers and expected that loading BA could endow the composite fibrous scaffold with the ability to regulate inflammation and promote vascularized bone regeneration. Besides, it was gratifying that core-shell structural fibers were also conducive to the sustained release of a drug, and the holes resulting from the degradation of FC could provide a channel for the release of BA [30]. The hydrophobility and slow degradation of PCL also made it useful for long-term delivery [31].

Here, we propose a core-shell structure fiber strategy (Scheme 1) using PLGA and PCL in combination to maximize their advantages and overcome their shortcomings. We investigated the anti-shrinkage performance of the coaxial fibrous scaffold in several common liquid media by shrinkage tests. We also experimentally tested the physico-chemical properties and BA release behavior. Furthermore, we assessed the proliferation and osteogenic differentiation of bone mesenchymal stem cells (BMSCs), and investigated the polarization of macrophages cultured on fabricated scaffolds *in vitro*. The foreign body reaction and angiogenic activity of the PFC/PCL-BA scaffold were determined through subcutaneous Implantation. Finally, we evaluated the vascularized bone regeneration ability of PFC/PCL-BA through a critical-sized calvarial bone defect model.

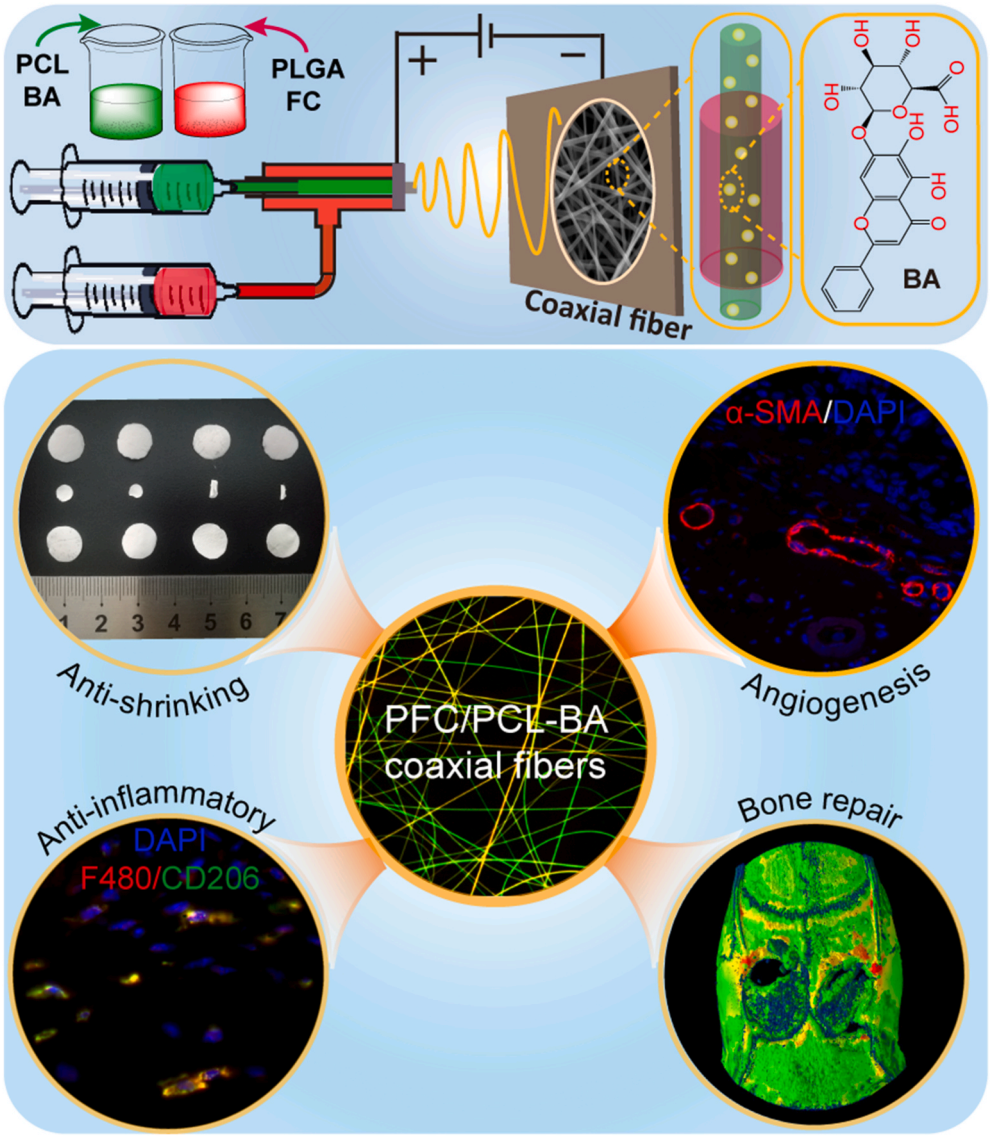

Scheme 1. The preparation schematic for PFC/PCL-BA coaxial fibrous scaffold and its remarkable multi-functions.

2. Experimental section

2.1. Materials and reagents

Poly-caprolactone (PCL, Mn = 80 kDa) was purchased from Shenzhen Esun Industrial Co., Ltd. (China). Poly (lactic-*co*-glycolic acid) (PLGA, LA/GA = 75:25, Mw = 105 kDa) was purchased from Jinan Daigang Biomaterial Co., Ltd. (China). Fish collagen (FC, from fish scale and skin) was purchased from Sangon Biotech Co., Ltd. (China). Baicalin (BA, $C_{21}H_{18}O_{11}$), Coumarin-6, 1,1,1,3,3,3-hexafluoro-2-isopropanol (HFIP) and 2,2,2-trifluoroethanol (TFE) were purchased from Aladdin Co., Ltd. (China). Rhodamine B was obtained from Beijing Solarbio Science & Technology Co., Ltd. (China). All other analytical reagents were supplied by Chengdu Kelong Co., Ltd. (China).

2.2. Fabrication of fibrous scaffold

All fibrous scaffolds were prepared using an electrospinning device (SS-2535, Beijing Ucalery Co., Ltd., China). Pure PCL and PCL-BA scaffolds were fabricated by a uniaxial flat-tipped needle. Core-shell nanofibers were fabricated by a coaxial needle. For preparing the PFC/PCL-BA scaffold, 0.08 g of FC and 0.4 g of PLGA were dissolved in 2 mL of HFIP and used as the outer coaxial needle solution. Considering that the degradation of PFC30 (30 wt %, FC to PLGA ratio) was too fast and PFC10 (10 wt %, FC to PLGA ratio) was relatively too slow, we chose optimal FC content as 20 wt % (FC to PLGA ratio) in the further study (Fig. S1). In addition, the uniform pores formed on the surface of PFC20 fibers during degradation may be conducive to drug release from the core-shell structural fibers (PFC/PCL-BA). Simultaneously, 0.12 g of PCL and 0.015 g of BA were dissolved in 1 mL of TFE and served as the inner coaxial needle solution. The flow rate of the outer solution and the inner solution during electrospinning were 0.32 mL/h and 0.16 mL/h, respectively. The theoretical mass ratio of BA in the final fibrous scaffolds was 2.5 wt %. A high voltage of 7 kV and a distance of 15 cm were applied between the syringe needle and the flat-collector. The preparation method of the core-shell fiber scaffold of PFC/PCL was like the method used for the PFC/PCL-BA scaffold. The Fourier Transform infrared spectroscopy (FTIR) was also performed to prove the fibrous membranes were fabricated successfully (Fig. S2).

2.3. Shrinkage test

All samples were cut into 10 mm diameter discs and then soaked in several common biological liquid media, i.e., phosphate buffer saline (PBS) solution, normal saline, 75% ethanol solution and culture medium (α-MEM; Gibco, USA). After immersion for 24h at 37 °C, all discs were collected, and the soaking solution on the surface of scaffolds was blotted up with the wiping paper; thereafter, drawing the outline of discs with a marking pen. Finally, and the area of every disc was measured by Adobe Photoshop CC. Scanning electron microscopy (SEM; JSM-6510LV, JEOL, Japan) was employed to observe fibrous scaffolds' morphology.

2.4. Characterization of nanofibrous scaffolds

The morphology of the nanofibrous scaffolds was observed by SEM. Transmission electron microscopy (TEM; Tecnai G2 F20, FEI, USA) was employed to observe the nanofibers' core-shell structure. To further determine the core and shell layer in the coaxial structure fibers, traces of fluorescent agents were mixed with the electrospun solution (Coumarin-6 in the shell layer and Rhodamine B in the core layer). Confocal laser scanning microscopy (CLSM; AIR MP^+, Nikon, Japan) was used to collect fluorescence images of the fibers. An electronic universal testing machine (AG-IC 50 KN, SHIMADZU, Japan) was applied to test the mechanical properties. All samples for mechanical properties tests were cut into a dumbbell shape. The scaffold's wettability was measured using a contact angle measuring instrument (JY-82 B, Chengde Dingsheng, China).

2.5. In vitro drug release

Three kinds of scaffold were used: 1) PCL-BA, uniaxial fibers; 2) P/PCL-BA, coaxial fibers, the shell layer was pure PLGA, and the core layer was PCL loaded with BA; and 3) PFC/PCL-BA, coaxial fibers (the shell layer was PLGA modified by FC, and the core layer was PCL loaded with BA). All samples were cut into thin slices of 15 mm in length and 10 mm in width. After that, they were immersed in a 15-mL centrifuge tube with 10 mL of PBS solution (pH 7.4) and placed in a thermostatic oscillator at 100 rpm and 37 °C. At a predetermined time-point, all of the released solutions were collected, and the fresh immersing solution was supplemented to 10 mL. The amount of released BA was measured by a fluorescence spectrometer (F-7000, Hitachi, Japan).

2.6. In vitro degradation behavior

The PCL, PFC, PFC/PCL and PFC/PCL-BA fibrous membranes were cut into rectangles with a length of 15 mm and a width of 10 mm and weighed accurately (recorded as M_0). Each membrane was put into a 5 mL plastic tube with 4 mL of PBS solution (pH = 7.4), respectively, and then all tubes were put in a shaking incubator at 120 rpm and 37 °C. The incubating media were replaced every week. At each preset time point, the samples were collected and dried to constant weight (recorded as M). SEM was performed to observe the morphology of fibers after degradation. The weight loss was determined according to the following formula:

$$Weight\ loss\ (\%) = \frac{M_0 - M}{M_0} \times 100\%$$

2.7. In vitro cell experiments

The proliferation and cytotoxicity of BMSCs cultured on scaffolds were investigated by Cell Counting Kit-8 (CCK-8; KeyGEN BioTECH, China) on days 1, 3 and 5. Hoechst 33342, Alexa Fluor® 546 phalloidin and Mito Tracker® Green FM were used to dye the BMSCs' nucleus, F-actin, and chondriosome, respectively, according to the manufactures' instructions (Life technologies, USA). The osteogenic differentiation gene expression (osteopontin, OPN; osteocalcin, OCN) of BMSCs cultured on the different scaffold for 14 days was tested by Real-Time PCR (RT-PCR) and calculated using the $2^{-\Delta\Delta CT}$ method. GAPDH was selected as the reference gene, and the relative gene expression for all samples was normalized by the control group (cells were cultured on a tissue culture plate). The primer sequences are listed in Table S1. The polarization of the macrophage cultured on different scaffolds after 3 days was investigated by flow cytometer. Macrophages (RAW264.7 cells) were first identified as $F4/80^+$ (BioLegend, USA), and the M2 macrophages were further identified by the marker of CD206 (BioLegend, USA).

2.8. Subcutaneous implantation

All experiments involving animals in this study were performed according to the normative guidelines and were approved by the ethics committee of Sichuan University (2020253 A). All experimental animals were anaesthetized with chloral hydrate before surgery. C57BL/6 mice aged 8 weeks were used to investigate the foreign body reaction and angiogenesis. PCL, PFC/PCL and PFC/PCL-BA fibrous scaffolds (3-mm diameter disc) were implanted into the back of each mouse, and the sham group (surgery only, no implanted material) was set up. All samples were collected when the mice were sacrificed at 1, 3, 7, and 14 days. Hematoxylin-Eosin (H&E) and immunofluorescence staining (F4/80, Servicebio; CD206, Abcam) were performed according to the

manufacturer's instructions.

2.9. Critical-sized calvarial bone defect repair

Two cylindrical defects (5 mm in diameter) were prepared on both sides of the Sprague-Dawley (SD) rat calvarial bone to evaluate bone regeneration. A fibrous membrane completely covered the defect area in the experimental group with a diameter of 8 mm. The sham group was without any implants. All SD rats were sacrificed after implantation for 4 and 8 weeks, and the neo-bone formation was analyzed by μ-CT (VivaCT80, SCANCO Medical AG, Switzerland) using 55 kV and 135 μA at high resolution. Those calvarial samples were decalcified by EDTA, and then, the H&E, tartrate-resistant acid phosphatase (TRAP), immunohistochemistry (Osterix, Abcam) and α-smooth muscle actin (α-SMA, Servicebio) fluorescence staining was performed.

2.10. Transcriptome sequencing and RT-PCR confirmation

Bulk RNA-Seq and RT-PCR of mouse calvarial bone was used to analyze the effect of BA on angiogenesis and bone formation/resorption-related gene expression. A 5-mm diameter defect was created on the middle seam of the calvarial bone. The bone defects were entirely covered by the PFC/PCL and PFC/PCL-BA fibrous scaffolds, respectively. Calvarial samples were collected and stored with RNA*later*™ stabilization solution (ThermoFisher Scientific, USA) after one week of implantation. Bulk-RNA-Seq was performed by Beijing Novogene Technology Co., Ltd. (China). We also further confirmed the key genes (*Pecam1, Vegfa, Tnfrsf11a* and *Ocstamp*) expression by RT-PCR utilizing calvarial bones. The primer sequences are listed in Table S1 and the β-actin was selected as the reference gene.

2.11. Statistical analysis

Data were expressed as means ± standard deviation of n = 3–6 replicates. One-way ANOVA with Tukey posttest in GraphPad InStat was used to analyze the significant difference between samples. The values were considered significantly different at $P < 0.05$. $^{*}p < 0.05$, $^{**}p < 0.01$ and $^{***}p < 0.001$; *NS*, no significant difference.

3. Results and discussion

3.1. Shape stability of core-shell structure fibrous scaffold

We evaluated the anti-shrinkage properties of the designed fibrous scaffold composed of PFC/PCL coaxial fibers by an immersion test (Fig. 1). Obviously, PCL and the core-shell structured PFC/PCL fibrous scaffold maintained their size and shape in general. However, PFC shrank and curled severely (Fig. 1a). The area maintenance ratios of the

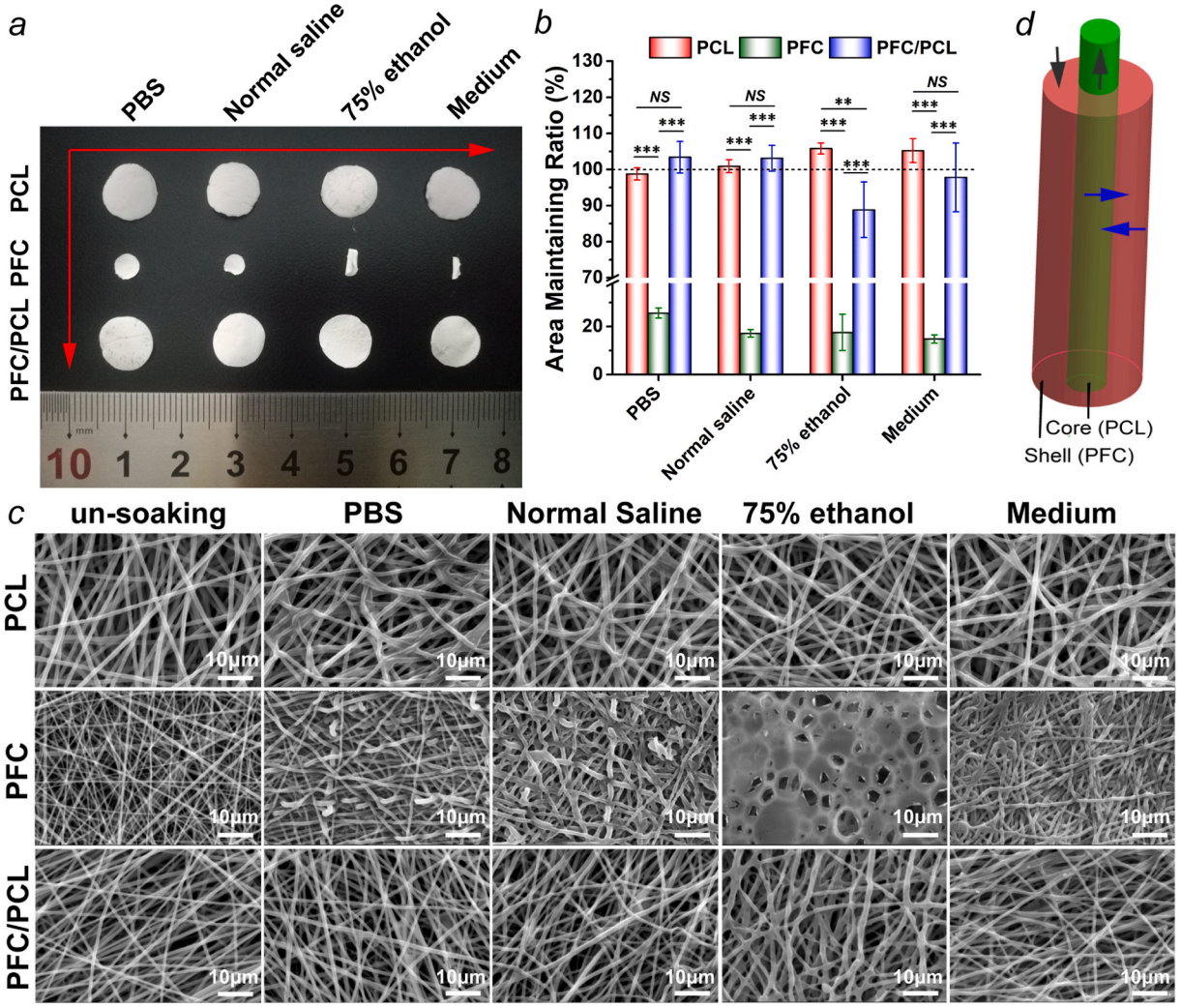

Fig. 1. a) The macroscopic photos of the fibrous scaffold after immersion in liquid media for 24 h; b) corresponding quantitative statistical analysis of the area maintaining ratio; c) SEM images of the fibrous scaffold before and after immersion; and d) schematic of the interaction between the core layer and the shell layer (black arrow, axial force; blue arrow, radial force).

PFC fibrous scaffold in four kinds of liquid media were less than 30% (Fig. 1b). In contrast, PCL had almost no change in dimension in PBS and normal saline, and even swelled slightly in 75% ethanol and medium. PFC/PCL fibrous scaffold maintained its size in PBS, normal saline, and medium (103.4 ± 4.4%, 103.1 ± 3.6% and 97.8 ± 9.5%, respectively), and shrank only mildly in 75% ethanol (88.8 ± 7.7%). Furthermore, we observed the morphology of these fibrous scaffolds after immersion by SEM (Fig. 1c). After immersion, only some PCL fibers were bent because of the stress relaxation in the fibers. The morphology of the coaxial PFC/PCL fibrous scaffold was like the morphology of PCL. However, due to the shrinkage of the PFC fibrous scaffold, the fibers became thicker, the pore was less structured, and the fiber network was denser. The PFC fibrous scaffold exhibited worse performance, as it almost completely lost the morphology of fibers and connected into one piece in 75% ethanol.

The dimensional stability of tissue engineering scaffolds is an essential condition for clinical application. The adverse changes (or even damage) to fiber morphology and pore structure caused by dimensional shrinkage were fatal to implanted fibrous materials. The dimensional shrinkage of materials would weaken their ability to maintain space and disturb cells' behavior on the implants [32]. Although PLGA has numerous merits, the shortcoming of its size shrinkage needed to be paid more attention to. Considering that the amorphous PLGA will shrink dramatically while the semi-crystalline PCL has a good stability of dimension, we utilized the characteristics of PCL and PLGA to combine them into core-shell structure fibers, thereby resisting the dimensional shrinkage through the axial and radial reverse interaction between them (Fig. 1d). Previous studies also provided some ideas to solve the shrinkage of PLGA, but the practicability of the existing strategies was limited [32,33]. For example, with degradation, the scaffold surface modified by plasma processing may gradually lose its dimensional stability, and the introduction of additional chemical components may cause cytotoxicity and reduce the biocompatibility of the scaffold. The results demonstrated that the PFC/PCL fibrous scaffold's core-shell structure could resist the dimensional shrinkage, as desired. Therefore, we further used the PFC/PCL coaxial fibrous scaffold as the drug carrier system in this study.

3.2. Morphology and coaxial structure of fibers

From Fig. 2a, we can see that the fibers of PCL, PFC/PCL and PFC/PCL-BA are randomly arranged, mimicking the typical structure of ECM. Compared with the PCL fibers, the diameter of the core-shell fibers decreased significantly (Fig. S3), mainly because the incorporation of FC and BA decreased the electrospinning solution's viscosity. In contrast to PCL-BA fibers, TEM images of PFC/PCL-BA fibers certified the core-shell structure (Fig. 2b and c). We further verified the coaxial fibers by fluorescence staining (Fig. 2d–g). CLSM images showed that the core and shell fibers were dyed red and green, respectively. The diameter of the core fiber was obviously smaller than the diameter of the coaxial fiber, and the coaxial fibers showed a yellow color derived by the mixing of red and green fluorescence. The high-resolution image also directly displayed the yellow color mainly distributed in the center of the fibers, indicating that the core-shell fiber was successfully fabricated. The core-shell structure of the fiber ensured the anti-shrinkage performance and was possibly beneficial to the sustained release of BA [34].

3.3. Mechanical properties and evaluation of wettability

Tensile tests were performed to evaluate the mechanical behavior of

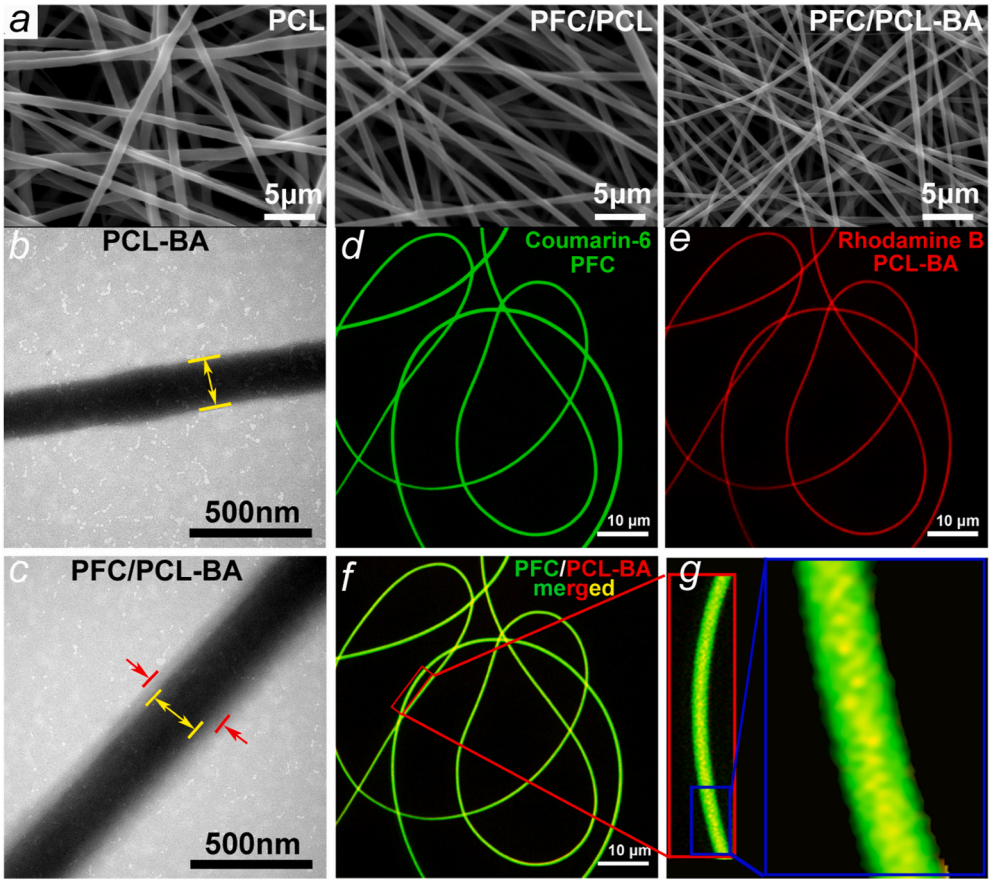

Fig. 2. a) SEM morphology of PCL, PFC and PFC/PCL-BA fibrous scaffold; b) TEM image of uniaxial PCL-loaded BA fiber and c) core-shell structure PFC/PCL-loaded BA fiber; d-g) The CLSM images of PFC/PCL-BA fibers.

the fibrous scaffold. Fig. 3a shows that the tensile behavior of PLGA, PFC/PCL and PFC/PCL-BA was similar, while the PCL fibrous scaffold had better elasticity. Concretely, the tensile strength of PCL fibrous scaffold reached 4.20 ± 0.25 MPa, which was significantly higher than the tensile strength of PLGA (3.22 ± 0.12 MPa) and PFC/PCL (3.59 ± 0.35 MPa). Importantly, there was no significant difference in the tensile stress of PFC/PCL-BA (3.89 ± 0.29 MPa) compared to PCL (Fig. 3b). This lack of difference was mainly attributed to the finer fiber diameter and the presence of FC, although the shell framework, PLGA, had lower tensile stress [20]. From Fig. 3c and d, the elastic modulus of PCL (14.65 ± 1.47 MPa) was significantly lower than the elastic modulus of PLGA, PFC/PCL and PFC/PCL-BA, but its elongation at break was dramatically higher than the elongation of PLGA, PFC/PCL and PFC/PCL-BA. In general, the PFC/PCL-BA coaxial fibrous scaffold showed high tensile stress, elasticity modulus and appropriate elongation ratio.

Most of the biomaterials implanted in bone defects need to bear complex compressive or tensile stress from the host tissue [35]. This property determines whether the biomaterials can perform their functions, such as providing space for tissue regeneration and conducting mechanical force [36]. In this study, PCL, as the framework of the core-shell fibers, provided tensile strength support for PFC /PCL-BA fibrous scaffold, as we designed. The moderate elasticity modulus and elongation at break of PFC/PCL-BA depended mainly on PLGA. Fortunately, the designed core-shell structure fibrous scaffold retained the admirable characteristics of PCL and PLGA, respectively. In addition, we found that BA loading had no adverse effect on the overall mechanical properties of the coaxial fibrous scaffold.

The hydrophilicity of the implant material directly determines the behavior of the host cells on the fabric. Moreover, the hydrophilicity of the material significantly affects the drug release process of the drug-loaded material system. As shown in Fig. 3e, the contact angle of the coaxial fibrous scaffold remained the same with the addition of BA but was slightly lower with the shell layer's addition.

3.4. The release behavior of BA in vitro

We prepared three fibrous scaffolds with different drug loading methods to study the release behavior of BA, and the results are presented in Fig. 3f. Evidently, although the PCL-BA scaffold was hydrophobic, water molecules can also infiltrate the thin fibers, so large amounts of BA can be released rapidly from the PCL fibers through a diffusion-based mode [37]. In contrast, P/PCL-BA showed a slower release profile, mainly because of the barrier effect of the fibres' core-shell structure [34]. However, the cumulative amount of BA released from the P/PCL-BA scaffold was only 73.2 ± 5.6% after 28 days of incubation. For the PFC/PCL-BA scaffold, the fibre's core-shell structure had a certain physical barrier effect on the diffusion of BA. The hydrophilic FC in the shell layer was more favorable to the infiltration of water molecular [20]. In addition, the FC was dissolved and diffused from the shell layer rapidly and then generated the holes in the surface of the PFC/PCL-BA fibers, thus providing a physical channel for the release of BA from the core layer. The cumulative amount of BA released from the PFC/PCL-BA scaffold reached 96.4 ± 1.6% at day 28, which was significantly higher than the cumulative amount of BA released from the P/PCL-BA (73.2 ± 5.6%), guaranteeing that the concentration of BA released from the PFC/PCL-BA scaffold after 14 days was still higher than the concentration of BA reported effective to promote ALP activity and mineralization [38]. The results demonstrated that BA's release mode in the PFC/PCL-BA fibrous scaffold was a combination of diffusion-based and degradation-based modes [39].

In this study, the designed coaxial PFC/PCL-BA fibrous scaffold was shown to achieve a continuous release of BA. The core-shell structure of fibers and the introduction of FC played a vital role in the release of BA. On the first day, there was a certain degree of burst release, followed by a sustainable release for nearly four weeks and the almost complete release of BA. The initial release of BA may be beneficial for regulating the immune cells' function and the expression of inflammatory cytokines to alleviate the acute inflammatory response after biomaterials implantation, providing a beneficial local immune microenvironment for bone tissue regeneration [40]. The release of BA in the middle and later stages is conductive to regulating the formation and resorption of bone.

3.5. Degradation behavior

The degradation property was of great importance for bone tissue engineering applications [41,42]. The degradation behavior of PCL, PFC, PFC/PCL and PFC/PCL-BA was shown in Fig. 4. The degradation rate of the neat PCL fibrous scaffold was the slowest, and the weight loss after 14 days of degradation was only 3.06 ± 0.75%. In contrast, the degradation rate of PFC fibrous scaffold was the fastest, with a weight loss of 22.13 ± 2.22% after 7 days of degradation, and 27.71 ± 1.03%

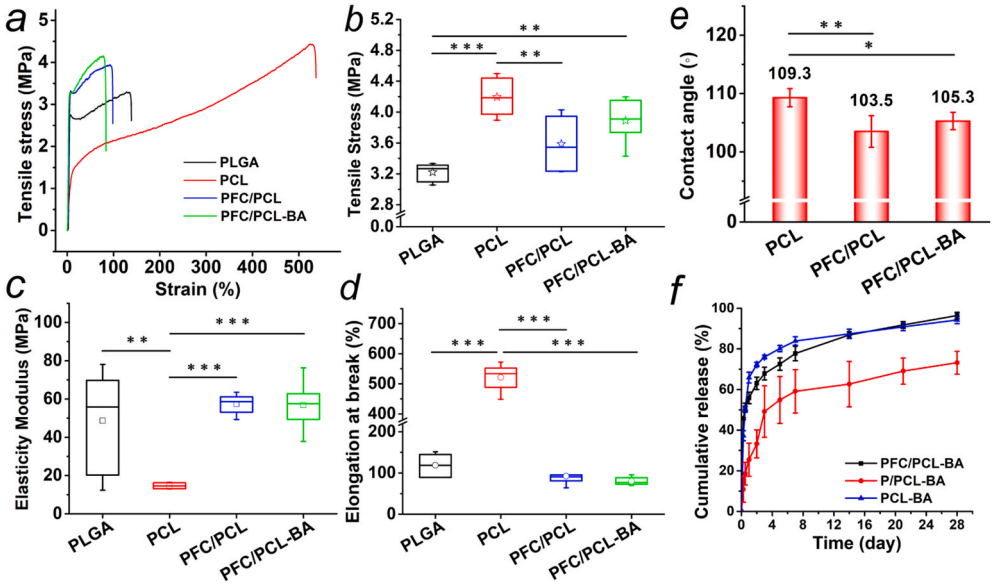

Fig. 3. Mechanical properties of fibrous scaffolds, a) typical strain-stress curve, b) tensile stress, c) elasticity modulus and d) elongation at break; e) Water contact angle of fibrous scaffolds; f) The release behavior of BA from PCL-BA, P/PCL-BA and PFC/PCL-BA fibrous scaffold.

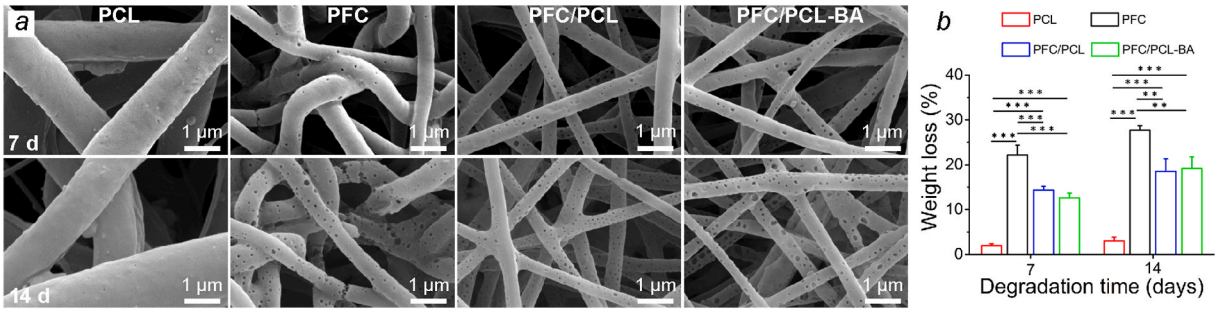

Fig. 4. Degradation behavior of fibrous scaffolds. a) The SEM images of PCL, PFC, PFC/PCL and PFC/PCL-BA fibrous scaffolds after degradation for 7 and 14 days; b) the corresponding weight loss of different fibrous scaffolds.

after 14 days. The core-shell structure of the fibrous membranes showed a relatively moderate degradation rate, and the drug in the core layer, BA, had no significant effect on the degradation behavior of the fibrous scaffold. In addition, it could be seen from the morphology of the degraded fibers that PFC, PFC/PCL and PFC/PCL-BA fibrous scaffolds showed a typical hole-like degradation, which was mainly caused by the rapid degradation of FC [20]. The PFC fiber was partially broken after 14 days of degradation, but PFC/PCL and PFC/PCL-BA fibers did not break, indicating that PCL could effectively maintain the stability of the core-shell structured fibrous scaffolds. The results of degradation experiments indicated that the presence of PCL could maintain the structural integrity and stability of the fibrous membranes, and the PFC of the shell layer could effectively accelerate the degradation rate of the whole fibrous scaffold.

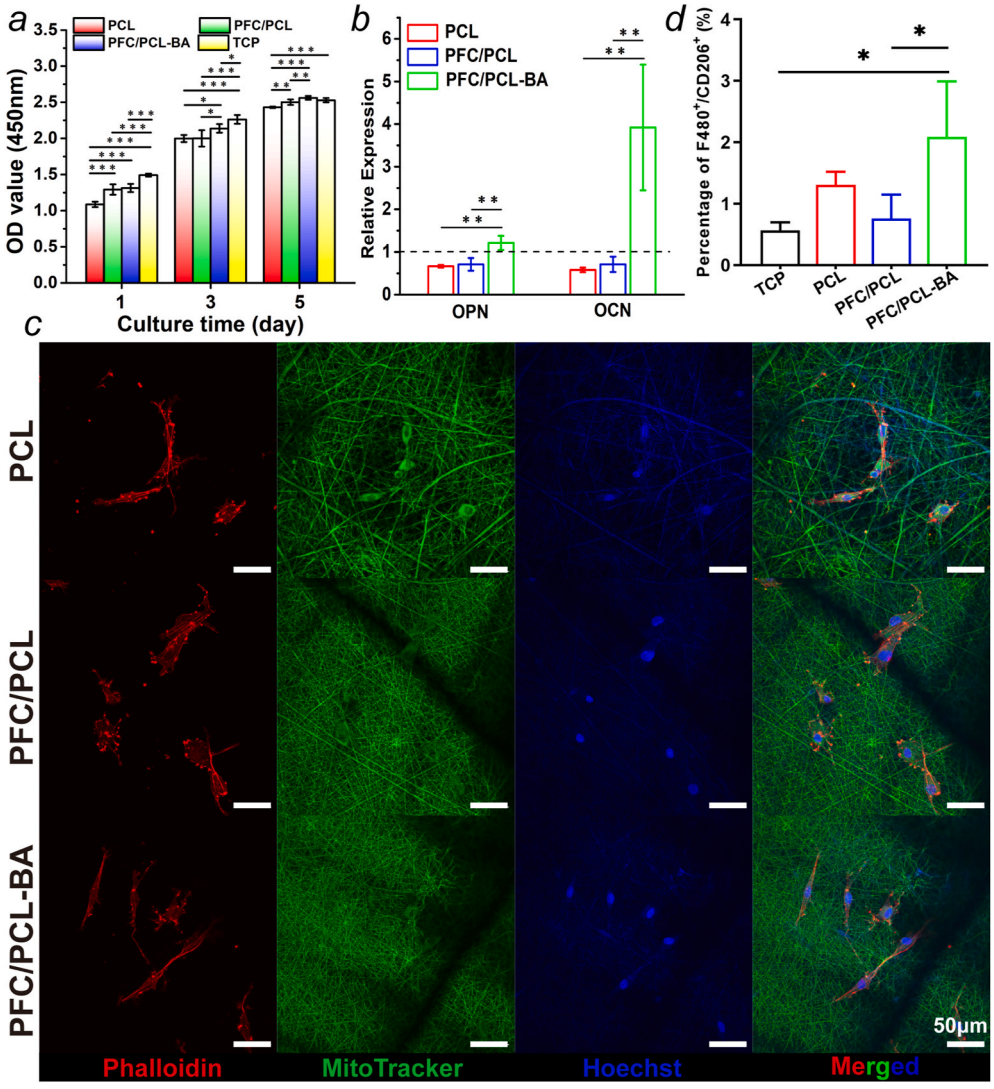

Fig. 5. The cell behavior of BMSCs and RAW264.7 on fibrous scaffolds. a) The proliferation of BMSCs on fibrous scaffolds; b) Relative expression of OPN and OCN genes in BMSCs cultured on fibrous scaffolds after 14 days; c) CLSM images of BMSCs cultured on fibrous scaffolds after 3 days; d) The polarization ratio of M2 phenotype ($F4/80^{+}$+$CD206^{+}$) after 3 days of culturing.

3.6. Cell viability and osteogenic differentiation of BMSCs

Both PLGA and PCL, as the framework of the designed coaxial fibers, were FDA-approved biocompatible biomedical polymers. FC was also recognized as a protein molecule with reliable bioactivity [43]. Therefore, the cell viability of the PFC/PCL-BA scaffold group depended mainly on the function of BA in the scaffold. We performed the CCK-8 assay to test the effect of the loaded BA on cell proliferation. As shown in Fig. 5a, the optical density (OD) value of the PFC/PCL and PFC/PCL-BA groups was significantly higher than the OD value of pristine PCL scaffold almost during the whole culturing process. These results indicated that PFC provided better cell attachment than PCL. Moreover, the difference between the PFC/PCL-BA and PFC/PCL groups increased gradually, contributing to the positive role of BA. Previous studies have shown that BA at a concentration greater than 50 μM can expedite cell viability [26]. Excitingly, there was no difference between the PFC/PCL-BA and the TCP group after 5 days of culturing. Taken together, the cell viability of BMSCs on the PFC/PCL-BA scaffold was significantly higher than the cell viability on other scaffolds. These results demonstrated that the design of the coaxial fibers and the presence of BA improved the cytocompatibility of the fibrous scaffold. Also, we detected the proliferation of BMSCs cultured on those scaffolds for 3 days by flow cytometry (Fig. S4), and the results corresponded to the CCK-8 assay. The F-actin microfilaments showed a long and thin morphology, indicating that the skeleton of BMSCs was intact and the cells spread adequately on the surface of the PFC/PCL and PFC/PCL-BA fibrous scaffolds (Fig. 5c). From these results, BA played an affirmative role in the proliferation of BMSCs, which was similar to the results from a previous study reported that BA could promote the proliferation of human ligament cells [44].

The effect of BA on the osteogenic differentiation of BMSCs *in vitro* was evaluated by detecting the expression of typical osteogenic differentiation markers. Fig. 5b shows the relative expression of the marker of early and late osteogenic differentiation, osteopontin (OPN) and osteocalcin (OCN), respectively. Notably, the expression of OPN and OCN was dramatically higher in BMSCs on the PFC/PCL-BA scaffold than on the PCL and PFC/PCL scaffolds. The Alizarin Red staining also showed that the PFC/PCL-BA scaffold had a better ability to promote osteogenic differentiation (Fig. S5). The *in vitro* experimental results demonstrated that BA in the scaffold could upregulate the expression of osteogenic related genes in BMSCs, which may be beneficial for accelerating bone regeneration. Previous studies also proved that BA could promote osteogenic differentiation by activating the Wnt/β-catenin pathway [26,45].

3.7. Polarization of RAW264.7 cells in vitro

The macrophage's polarization is considered as an important biological process in foreign body reaction and tissue repair [46,47]. Typically, macrophages exhibit pro-inflammatory (M1 phenotype) and pro-reparative (M2 phenotype) polarization phenotypes in the interaction with implant materials and the regulation of the local immune microenvironment [48,49]. In this study, we observed the morphology of RAW264.7 cells, and further assessed the number of M2 phenotype cultured on scaffolds after 3 days. More M2 macrophage phenotypes with elongated morphology emerged on the PFC/PCL-BA scaffold (Fig. S6). The positive expression of the $F4/80^{+}$and $CD206^{+}$ (M2) cell ratio on TCP, PCL, PFC/PCL and PFC/PCL-BA was 0.57 ± 0.13%, 1.3 ± 0.21%, 0.76 ± 0.39% and 2.09 ± 0.9%, respectively (Fig. 5d). The percentage of RAW264.7 cells polarized to the M2 phenotype on the PFC/PCL-BA scaffold was significantly higher than the percentage of RAW264.7 cells polarized to the M2 phenotype on the TCP and the PFC/PCL group. Xu et al. demonstrated that BA could also switch macrophages' polarization from M1 to M2 *in vivo* [50]. These results showed that BA played a positive role in regulating macrophage polarization to a pro-reparative phenotype, which provided a basis for creating the local immune microenvironment to promote tissue regeneration.

3.8. In vivo evaluation of foreign body reaction

Foreign body reaction is a series of complex reaction of host tissue to resist excessive physiological response and stimulation caused by infection. The magnitude of the stress response of immune cells induced by implanted material plays a crucial role in material-mediated tissue repair [51]. The foreign body reaction caused by the prepared scaffolds implanted subcutaneously into mice is shown in Fig. 6. Obviously, many immune cells were recruited around those fibrous scaffolds and the sham group after 1 day of implantation. Remarkably, there were more inflammatory cells around the PCL scaffold compared with the PFC/PCL and PFC/PCL-BA scaffolds, which lasted until 14 days after implantation. In a worse reaction, there were thick collagenous fibrosis capsules around the PCL scaffold but not around the PFC/PCL and PFC/PCL-BA scaffolds at 14 days. Due to the homeostasis regulation of host tissue, the inflammation around PFC/PCL and PFC/PCL-BA scaffolds was gradually relieved. Immune cells interacted with the coaxial fibrous scaffold, some cells infiltrated into the scaffold, and the scaffold degraded mildly. Many foreign body giant cells formed around the PCL scaffold, showing a chronic inflammatory response, which was similar to results from previous studies [19].

More importantly, 14 days after implantation, we observed that there were mature blood vessels around the PFC/PCL-BA scaffold, and there were some blood capillaries in the PFC/PCL and sham group. In contrast, almost no neovascularization occurred in the PCL group. This result was further confirmed by fluorescence staining of CD31 and α-SMA (Fig. S7). This may benefit from the excellent biological activity of BA and FC in the coaxial fibers. The coaxial structure fibrous scaffold performed well in the moderation of the local microenvironment. Of course, BA also played an anti-inflammatory role and inhibited the fibrosis role in the whole process of foreign body reaction [52–54]. Previous research has shown that BA could regulate anti-inflammation through the miR-124-STAT3 signaling pathway [55]. The immunofluorescence staining showed that a large number of macrophages ($F4/80^{+}$) were recruited around fibrous scaffolds one day after implantation, indicating the occurrence of an early acute inflammatory reaction, which weakened after 14 days (Fig. 7). Obviously, the PFC/PCL-BA group showed more pro-reparative macrophages ($F4/80^{+}$ and $CD206^{+}$) than the PCL and PFC/PCL group. In general, the designed PFC/PCL-BA scaffold can create a pro-regenerative immune microenvironment by regulating the macrophage phenotype transition.

3.9. Bone regeneration evaluation via critical-sized calvarial bone defect model

The capacity of the PCL, PFC/PCL and PFC/PCL-BA scaffolds to guide bone regeneration was investigated in SD rats with the critical-sized calvarial bone defect model. We analyzed the formation of new bone and the spatial structure of bone trabecula by μ-CT scanning analysis at 4 weeks and 8 weeks (Fig. 8) after implantation. At 4 weeks after surgery, the BV/TV of PFC/PCL-BA was significantly higher than the BV/TV of the sham and PCL group. The trabecular connection density (Conn.D.) was also higher in the PFC/PCL-BA group than the PCL group and the sham group. The trabecular number (Tb.N) of the PFC/PCL-BA group was obviously higher than that of other groups. The trabecular separation (Tb.Sp) of PFC/PCL-BA group was lower than the Tb.Sp of the sham and PCL group. After 8 weeks of implantation, we observed that the BV/TV of the PFC/PCL-BA group was remarkably higher than the BV/TV of the PFC/PCL, PCL and sham group. Similarly, the Tb.N of the PFC/PCL-BA group was dramatically higher than other groups. A lower value of the Tb.Sp was found in the PFC/PCL-BA group compared with both the PFC/PCL and the sham groups.

The volume fraction of bone directly reflects the formation of new

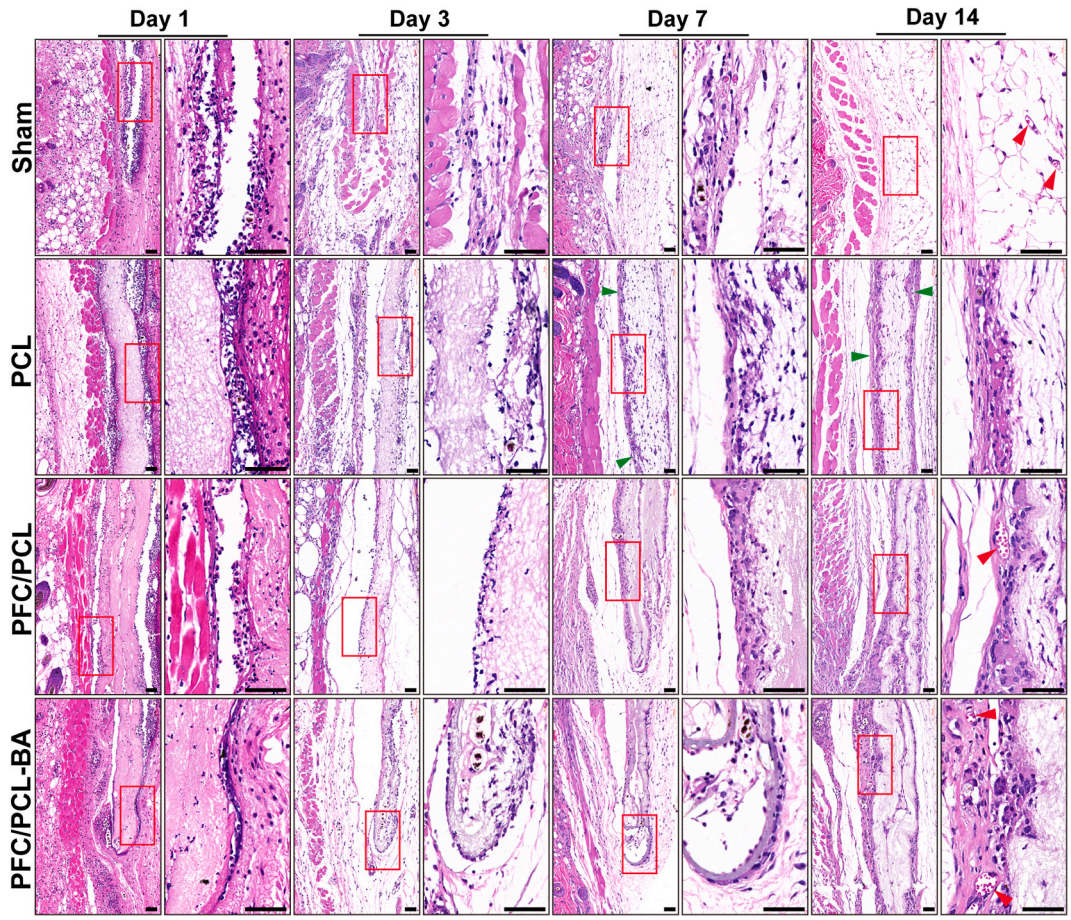

Fig. 6. Representative H&E staining images of subcutaneous implantation after 1, 3, 7 and 14 days; the image on the right is the corresponding high magnification image of the red box on the left. The red arrow indicates blood vessels, the green arrow indicates fibrosis location, and the black scale bar represents 50 μm.

bone. The trabecular microarchitecture can also show the progress of bone regeneration and the health of new bone [56]. After 4 weeks of implantation, the overall osteogenic effect of the PFC/PCL-BA group was significantly higher than other groups. Although there was no significant difference in BV/TV between the PFC/PCL-BA group and the PFC/PCL group, the Tb.N in the PFC/PCL-BA group was higher than the Tb.N in the PFC/PCL group. It was satisfactory that the PFC/PCL-BA group distinctly overmatched other groups in both BV/TV and trabecular spatial microarchitecture parameters after 8 weeks implantation, which may be due to the increase in bone formation by osteoblasts and the decrease in bone resorption by osteoclasts at the trabecular surface [57]. The results demonstrated that the PFC/PCL-BA scaffolds could guide bone regeneration as desired, and BA in the scaffold may promote bone regeneration by enhancing the microarchitecture of the trabeculae. BA provided a beneficial immune microenvironment for bone regeneration by regulating pro/anti-inflammatory mediators in the early implantation stage. Then, BA further regulated bone remodeling by the osteoblast-mediated bone formation and osteoclast-mediated related bone resorption [58,59]. Besides, we found that the unmodified PCL and PFC-modified PCL scaffolds did not show a satisfactory bone regeneration effect. This result indicates that, in the absence of osteogenic induction cues, the PCL and the PFC/PCL scaffolds only acted as a barrier to provide space for osteogenesis without sufficient osteoinductivity, but this effect was limited in the critical-sized calvarial bone defect model of SD rats, consistent with the results reported in other studies. Zha et al. showed that the coaxial chitosan/PLA nanofibrous scaffold lacked the ability for promotion of bone formation in rat cranial defects repair [21]. Other experimental results also showed that PLGA-collagen-gelatin-bioactive glass hybrid nanofiber aerogels did not perform well in bone regeneration [60]. This suggested that the introduction of osteogenic clues was critical in the design of polymer-based bone regeneration scaffolds.

3.10. Histological analysis

The bone formation and neovascularization were further investigated by histomorphological analysis following H&E, Masson (Fig. S9), immunohistochemistry and immunofluorescence staining, as shown in Fig. 9. At 4 weeks postimplantation, there was newly formed bone in the center of the defect area in the PFC/PCL-BA group, and a relatively smaller new bone area was observed in the PFC/PCL group. By contrast, the newly formed bone in the PCL and sham groups was mainly located at the periphery of the defect in a limited amount and surrounded by fibrous connective tissue. A large amount of dense new bone tissue was formed in the PFC/PCL-BA group, and the defect area was almost wholly closured at 8 weeks after implantation. In contrast, the PFC/PCL, PCL, and sham groups formed new bone in the defect's middle region without integrally bridging in the defect site. During the bone regeneration, we did not observe evident inflammation in all groups except the PCL group. We also further confirmed the expression of transcription activator (Osterix) essential for osteoblast differentiation at 8 weeks (Fig. 9c and f). Compared with other groups, the PFC/PCL-BA group had more Osterix-positive expression cells, indicating that the PFC/PCL-BA fibrous scaffold created a more favorable osteogenic microenvironment. Moreover, all the fibrous scaffolds were not entirely degraded, and the macroscopic integrity of the scaffold was maintained (Fig. S10), which indicated that the degradation rate of the designed coaxial fibrous scaffold could meet the requirement of guided bone regeneration. Most

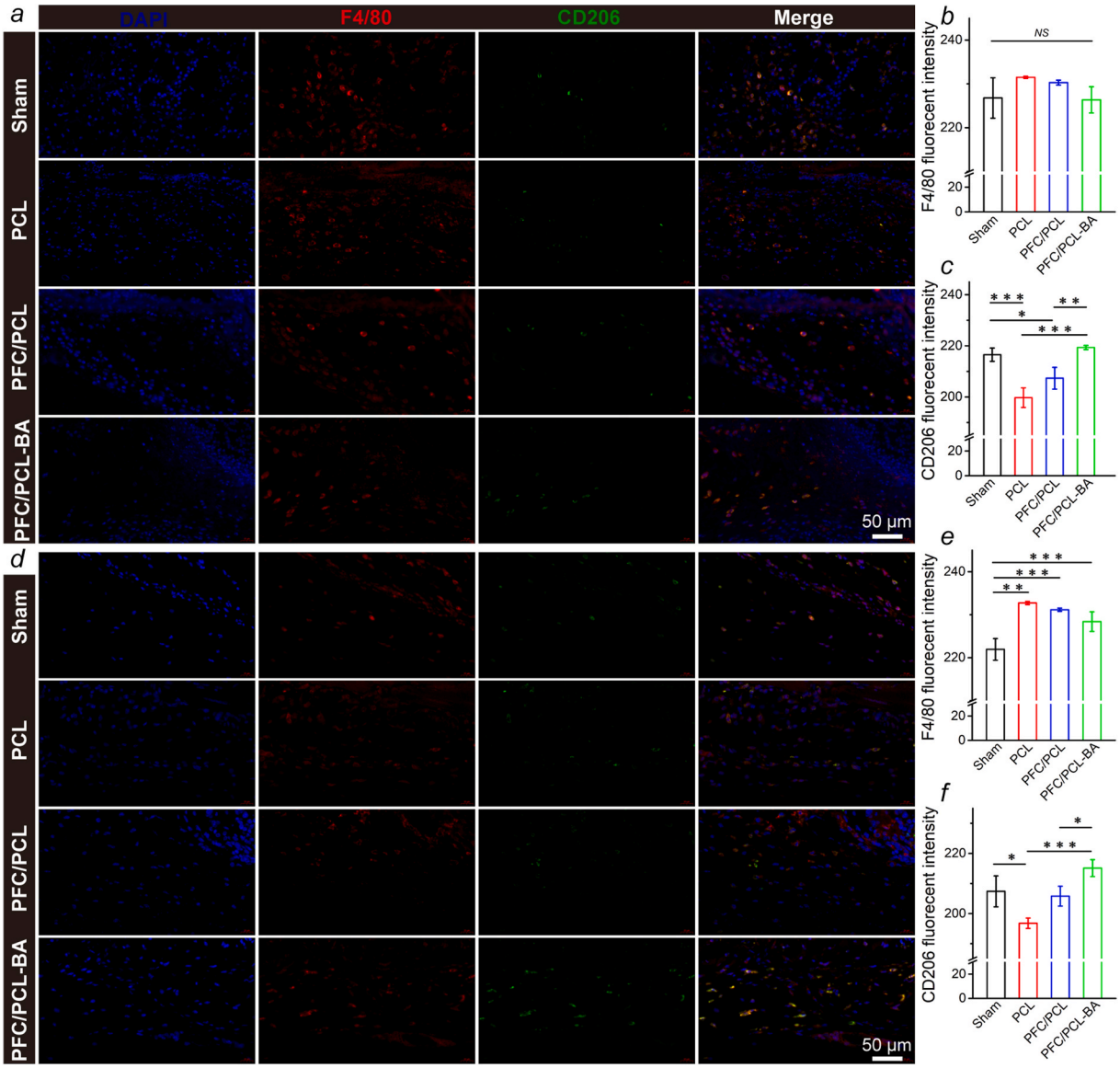

Fig. 7. Immunofluorescence staining of the macrophages around different scaffolds. The positive expression and fluorescent intensity of F4/80 and CD206 after 1d (a, b and c) and 14d (d, e and f) subcutaneous implantation.

importantly, we found that mature blood vessels formed within the new bone in the PFC/PCL-BA group after 8 weeks, whereas only a small number of newly developing capillaries were found in the PFC/PCL and PCL groups. The fluorescence staining also confirmed the formation of neovascular in the new bone tissue (Fig. 9d and e). The positive expression of blood vessel marker (α-SMA) in the PFC/PCL-BA group was significantly higher than that in other groups.

We further investigated the balance of the bone regeneration process by TRAP staining markers of osteoclasts. The PFC/PCL, PCL and sham groups showed obviously positive expression of TRAP (Fig. 9b, g and h) at 4 and 8 weeks; however, the PFC/PCL-BA group only exhibited the positive expression of TRAP at 8 weeks after implantation, suggesting that the coaxial fibrous scaffold loaded with BA can significantly inhibit the osteoclast activity in early osteogenesis. Compared with other groups, the PFC/PCL-BA group presented a highly retarded bone resorption during the regeneration. Interestingly, we found that the TRAP-positive region in the PFC/PCL-BA group was precisely where the neovascularization occurred, indicating that osteoclasts provide channels for blood vessels' formation. These results explained that the TRAP activity of the PFC/PCL-BA group was significantly higher than that of the Sham and PFC/PCL group at 8 weeks. It was the coupling of angiogenesis and osteoclast differentiation that promoted functional bone regeneration in the defect area. These results suggested that we have successfully constructed a BA-loaded coaxial fibrous scaffold to mediate vascularized bone regeneration.

3.11. *Bulk-RNA-seq*

Finally, the role of BA in bone regeneration was preliminarily investigated using the RNA-Seq of mouse calvarial defect samples. According to each sample's distribution in the 2D principal component analysis (PCA) graph, the RNA expression profiles of the PFC/PCL and PFC/PCL-BA groups were obviously different (Fig. 10a). We further validated the expression of the key genes associated with angiogenesis and osteoclast differentiation. An angiogenesis heatmap showed the positive regulation of vascular sprout-, development- and maturation-related genes (Fig. 10b). For example, *Vegfa*, involving angiogenesis and endothelial cell growth, was significantly upregulated in the PFC/PCL-BA group compared to the PFC/PCL group. Likewise, *Angpt1* and *Angpt4,* which activate PTK2/FAK and the downstream kinases and

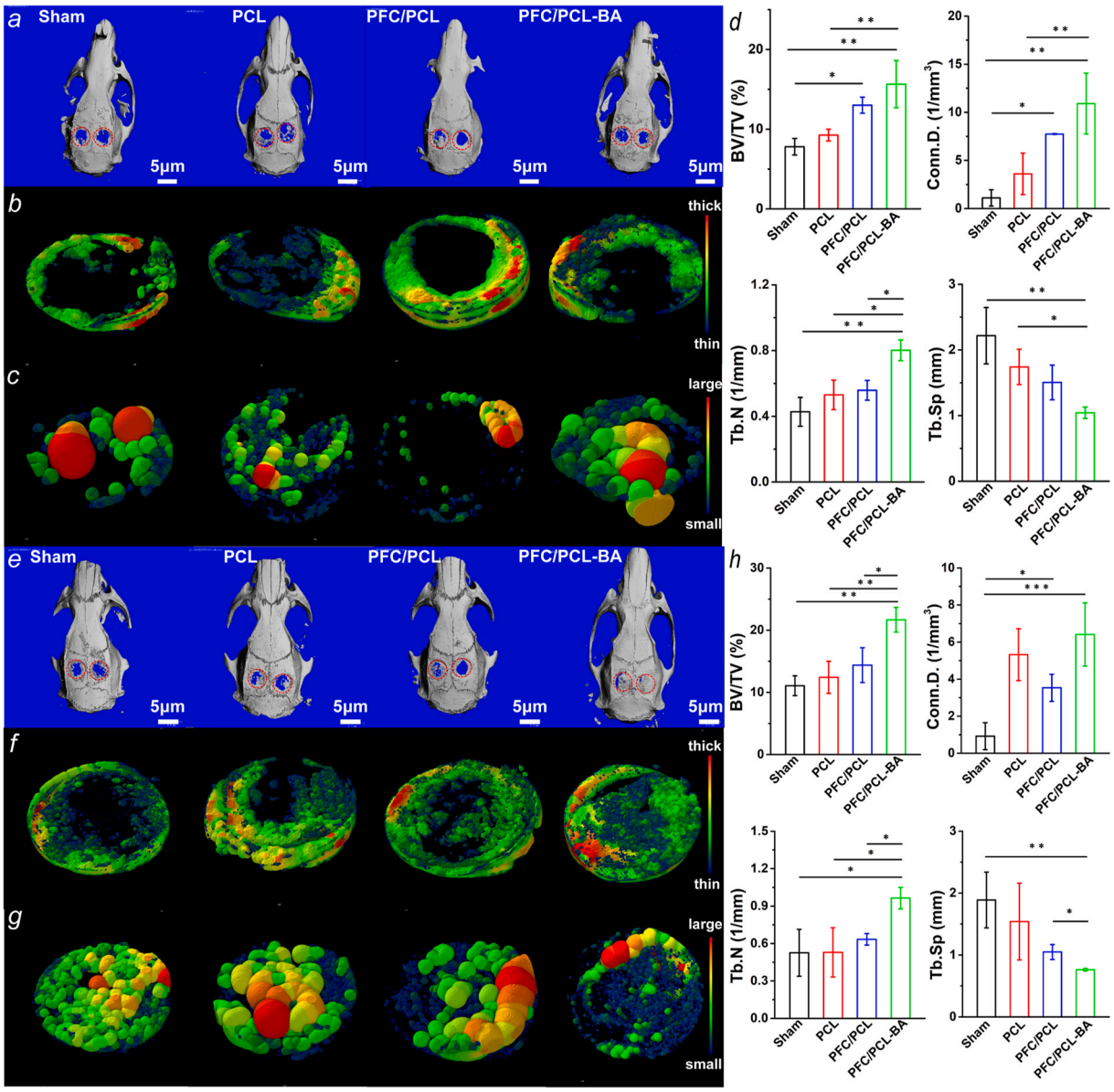

Fig. 8. The repair effect of rat calvarial bone after 4 weeks of implantation: a) μ-CT panoramic view of the rat calvarial bone; b) Images of neo-bone and trabecular thickness (Tb.Th) distribution in the defect area; c) Images of Tb.Sp in the defect area; d) Quantitative analysis of BV/TV, Conn.D., Tb.N and Tb.Sp; e-h) The corresponding repair effect of rat calvarial bone after 8 weeks of implantation. The reconstructed micro-CT images of defect site were also provided in supporting information (Fig. S8).

ultimately stimulate sprouting angiogenesis, also showed high expression in the PFC/PCL-BA group. The expression of other blood vessel development- and maturation-related genes in the PFC/PCL-BA group was also higher than in the PFC/PCL group, indicating that BA played an active role in vascularization. We further confirmed the gene expression of angiogenesis-related regulators by RT-PCR (Fig. 10c). The results showed that the *Pecam1* and *Vegfa* were significantly upregulated in the PFC/PCL-BA group. The osteoclast differentiation heatmap represented the gene expression of the positive and negative regulation of osteoclast differentiation or bone resorption (Fig. 10d). Remarkably, the genes expression of the negative regulation of osteoclast formation and differentiation were upregulated in the PFC/PCL-BA group compared to the PFC/PCL group; however, the positive regulation of the osteoclast differentiation was just the opposite. We noted that the expression of *Tnfsf11*, which induces osteoclastogenesis by activating multiple signaling pathways in the osteoclast precursor cells, was downregulated in the PFC/PCL-BA group. Similarly, the *Tnfrsf11a* was essential for RANKL-mediated osteoclastogenesis and was also downregulated in the PFC/PCL-BA group. RT-PCR results also confirmed that *Tnfrsf11a* gene expression was significantly downregulated in the PFC/PCL-BA group, although there was no significant difference in *Ocstamp* gene expression (Fig. 10e). Therefore, compared with the PFC/PCL group, BA indeed suppressed osteoclast formation and differentiation in early osteogenesis. Overall, the results demonstrated that the PFC/PCL-BA scaffold could motivate angiogenesis and inhibit osteoclast differentiation, thereby promoting bone regeneration.

4. Conclusion

This work describes a simple, feasible and effective approach to overcome the shortcomings of PLGA and PCL electrospun fiber. We demonstrated that the core-shell structure fibrous scaffold could effectively inhibit the shrinkage of PLGA. This strategy overcomes the weakness of PLGA-based fibrous scaffolds and expands its application in

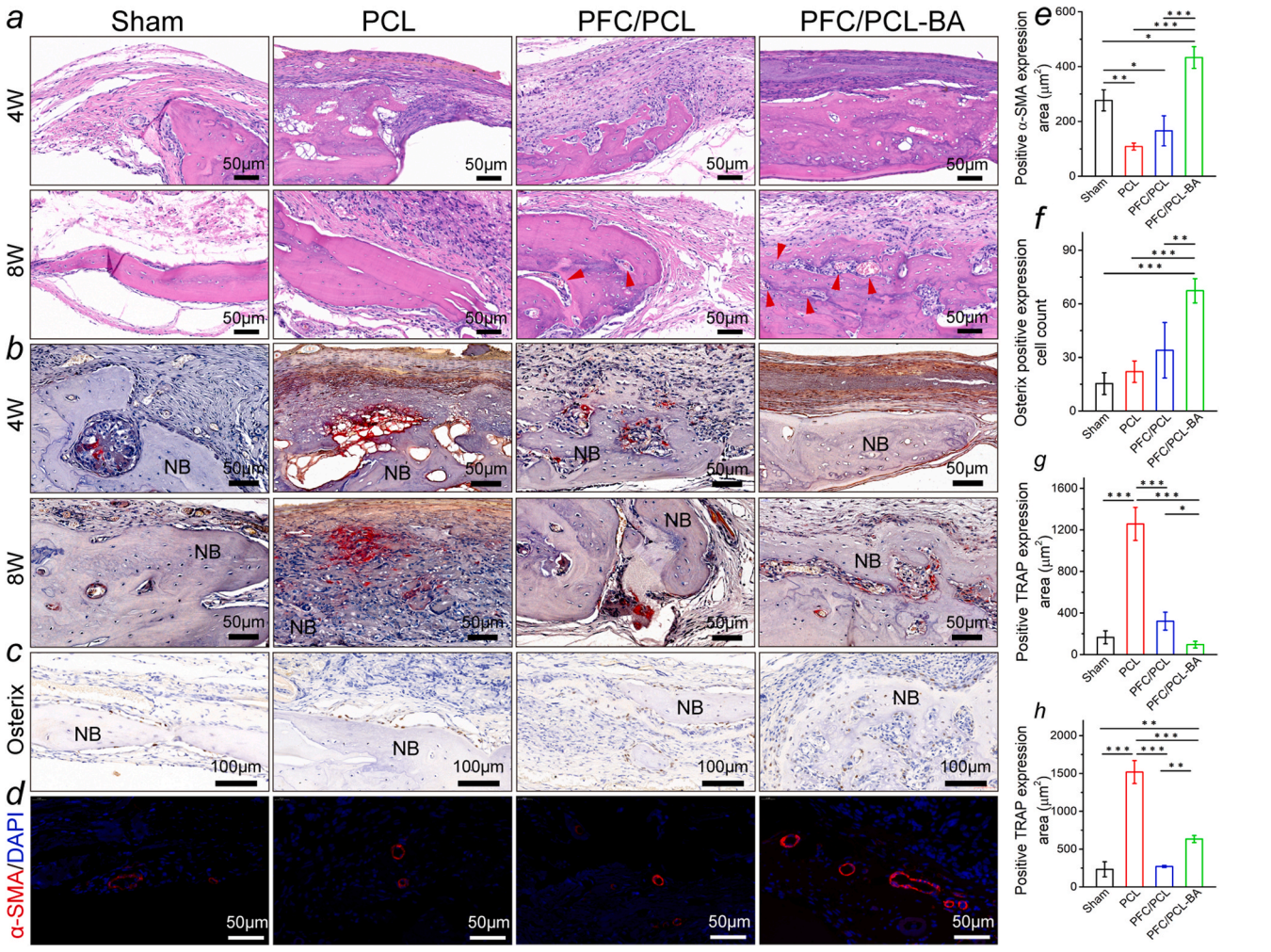

Fig. 9. Histological section analysis: a) H&E staining; b) TRAP staining of calvarial bone samples and corresponding semi-quantitative statistics (g, 4 weeks; h, 8 weeks); c) the immunohistochemistry staining of osteoblast differentiation-related transcription activator (Osterix) and corresponding semi-quantitative statistics (f) at 8 weeks post-implantation; d) the fluorescence staining of blood vessels (α-SMA/DAPI) and corresponding semi-quantitative statistics (e) at 8 weeks post-implantation. The red arrows in the H&E images indicate blood vessels; NB, newly formed bone.

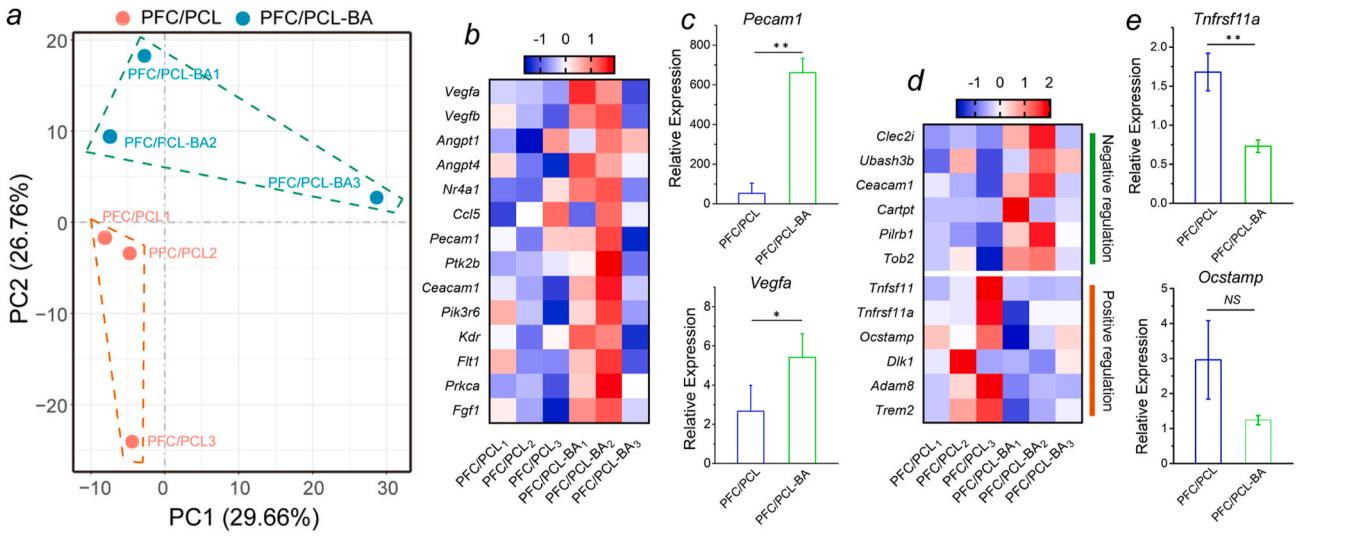

Fig. 10. RNA expression levels after 1 week of implantation determined utilizing Bulk-RNA-Seq and RT-PCR. a) The 2D PCA of RNA expression profile in PFC/PCL and PFC/PCL-BA, respectively; b) Heatmap representing the expression of angiogenesis-related regulators; c) Detection of gene expression of key angiogenesis-related regulators (*Pecam1* and *Vegfa*) by RT-PCR; d) Heatmap representing the expression of positive and negative regulators of osteoclast differentiation; e) Detection of gene expression of osteoclast differentiation-related regulators (*Tnfrsf11a* and *Ocstamp*) by RT-PCR.

bone tissue engineering. The PFC/PCL-BA scaffold exhibited good comprehensive mechanical properties and the ability to release BA continuously. The presence of BA did not cause cytotoxicity and significantly promote the osteogenic differentiation of BMSCs *in vitro*. Moreover, the PFC/PCL-BA scaffold could mediate anti-inflammatory response by regulating the macrophage phenotype transition. Most importantly, the PFC/PCL-BA scaffold remarkably promoted functional bone formation with favorable trabecular microarchitecture and vascular network by enhancing angiogenesis and regulating osteoclast differentiation. Taken together, this work strongly supports that the effectiveness of dimensionally stable core-shell structured fiber as a drug release platform, which was a promising candidate for vascularized bone regeneration.

CRediT authorship contribution statement

Shue Jin: Data curation, Writing – original draft, Investigation. **Jing Gao:** Investigation. **Renli Yang:** Writing – review & editing. **Chen Yuan:** Data curation. **Ruili Wang:** Writing – review & editing. **Qin Zou:** Visualization, Methodology. **Yi Zuo:** Supervision, Methodology. **Meifang Zhu:** Project administration, Funding acquisition. **Yubao Li:** Project administration, Conceptualization, Funding acquisition. **Yi Man:** Supervision. **Jidong Li:** Conceptualization, Methodology, Writing – review & editing.

Declaration of competing interest

The authors declare no conflict of interest.

Acknowledgments

This work was supported by the National Key Research and Development Program of China (No.2016YFA0201703/2016YFA0201700) and the Key R&D Project of Sichuan Science and Technology Plan (2021YFS0030). We would like to thank Doctor Chenghui Li and Li Chen from Analytical & Testing Center, Sichuan University for the help with CLSM and μ-CT images, respectively. We appreciate Doctor Fang Yang's suggestion of this work.

Appendix A. Supplementary data

Supplementary data to this article can be found online at https://doi.org/10.1016/j.bioactmat.2021.06.028.

References

[1] A.R. Armiento, L.P. Hatt, G. Sanchez Rosenberg, K. Thompson, M.J. Stoddart, Functional biomaterials for bone regeneration: a lesson in complex biology, Adv. Funct. Mater. 30 (2020) 1909874.
[2] G. Yang, H. Liu, Y. Cui, J. Li, X. Zhou, N. Wang, F. Wu, Y. Li, Y. Liu, X. Jiang, S. Zhang, Bioinspired membrane provides periosteum-mimetic microenvironment for accelerating vascularized bone regeneration, Biomaterials 268 (2020) 120561.
[3] R. Subbiah, M.P. Hwang, S.Y. Van, S.H. Do, H. Park, K. Lee, S.H. Kim, K. Yun, K. Park, Osteogenic/angiogenic dual growth factor delivery microcapsules for regeneration of vascularized bone tissue, Adv. Healthcare. Mater. 4 (2015) 1982–1992.
[4] S. Li, C. Song, S. Yang, W. Yu, W. Zhang, G. Zhang, Z. Xi, E. Lu, Supercritical CO2 foamed composite scaffolds incorporating bioactive lipids promote vascularized bone regeneration via Hif-1 alpha upregulation and enhanced type H vessel formation, Acta Biomater. 94 (2019) 253–267.
[5] A.S. Silva, L.F. Santos, M.C. Mendes, J.F. Mano, Multi-layer pre-vascularized magnetic cell sheets for bone regeneration, Biomaterials 231 (2020) 119664.
[6] C. Feng, J. Xue, X. Yu, D. Zhai, R. Lin, M. Zhang, L. Xia, X. Wang, Q. Yao, J. Chang, C. Wu, Co-inspired hydroxyapatite-based scaffolds for vascularized bone regeneration, Acta Biomater. 119 (2021) 419–431.
[7] W. Ji, F. Yang, H. Seyednejad, Z. Chen, W.E. Hennink, J.M. Anderson, J.J. van den Beucken, J.A. Jansen, Biocompatibility and degradation characteristics of PLGA-based electrospun nanofibrous scaffolds with nanoapatite incorporation, Biomaterials 33 (2012) 6604–6614.
[8] Y. Lai, Y. Li, H. Cao, J. Long, X. Wang, L. Li, C. Li, Q. Jia, B. Teng, T. Tang, J. Peng, D. Eglin, M. Alini, D.W. Grijpma, G. Richards, L. Qin, Osteogenic magnesium incorporated into PLGA/TCP porous scaffold by 3D printing for repairing challenging bone defect, Biomaterials 197 (2019) 207–219.
[9] F. Danhier, E. Ansorena, J.M. Silva, R. Coco, A. Le Breton, V. Preat, PLGA-based nanoparticles: an overview of biomedical applications, J. Contr. Release 161 (2012) 505–522.
[10] D. Hernan Perez de la Ossa, A. Ligresti, M.E. Gil-Alegre, M.R. Aberturas, J. Molpeceres, V. Di Marzo, A.I. Torres Suarez, Poly-epsilon-caprolactone microspheres as a drug delivery system for cannabinoid administration: development, characterization and in vitro evaluation of their antitumoral efficacy, J. Contr. Release 161 (2012) 927–932.
[11] Z. Wang, R. Liang, X. Jiang, J. Xie, P. Cai, H. Chen, X. Zhan, D. Lei, J. Zhao, L. Zheng, Electrospun PLGA/PCL/OCP nanofiber membranes promote osteogenic differentiation of mesenchymal stem cells (MSCs), Mater. Sci. Eng., C 104 (2019) 109796.
[12] S. Jin, X. Xia, J. Huang, C. Yuan, Y. Zuo, Y. Li, J. Li, Recent advances in PLGA-based biomaterials for bone tissue regeneration, Acta Biomater. 127 (2021) 56–79.
[13] X. Zhou, Q. Cai, N. Yan, X. Deng, X. Yang, In vitro hydrolytic and enzymatic degradation of nestlike-patterned electrospun poly(D,L-lactide-co-glycolide) scaffolds, J. Biomed. Mater. Res. 95 (2010) 755–765.
[14] J.B. Lee, Y.-G. Ko, D. Cho, W.H. Park, B.N. Kim, B.C. Lee, I.-K. Kang, O.H. Kwon, Modification of PLGA nanofibrous mats by electron beam irradiation for soft tissue regeneration, J. Nanomater. 2015 (2015) 1–10.
[15] X. Zong, S. Ran, K.-S. Kim, D. Fang, B.S. Hsiao, B. Chu, Structure and morphology changes during in vitro degradation, Biomacromolecules 4 (2003) 416–423.
[16] H.N. Chia, B.M. Wu, High-resolution direct 3D printed PLGA scaffolds: print and shrink, Biofabrication 7 (2014), 015002.
[17] A. Nasajpour, S. Ansari, C. Rinoldi, A.S. Rad, T. Aghaloo, S.R. Shin, Y.K. Mishra, R. Adelung, W. Swieszkowski, N. Annabi, A. Khademhosseini, A. Moshaverinia, A. Tamayol, A multifunctional polymeric periodontal membrane with osteogenic and antibacterial characteristics, Adv. Funct. Mater. 28 (2018) 1703437.
[18] S. Cheng, Y. Jin, N. Wang, F. Cao, W. Zhang, W. Bai, W. Zheng, X. Jiang, Self-adjusting, polymeric multilayered roll that can keep the shapes of the blood vessel scaffolds during biodegradation, Adv. Mater. 29 (2017) 1700171.
[19] Y. Qian, L. Li, Y. Song, L. Dong, P. Chen, X. Li, K. Cai, O. Germershaus, L. Yang, Y. Fan, Surface modification of nanofibrous matrices via layer-by-layer functionalized silk assembly for mitigating the foreign body reaction, Biomaterials 164 (2018) 22–37.
[20] S. Jin, F. Sun, Q. Zou, J. Huang, Y. Zuo, Y. Li, S. Wang, L. Cheng, Y. Man, F. Yang, J. Li, Fish collagen and hydroxyapatite reinforced poly(lactide- co-glycolide) fibrous membrane for guided bone regeneration, Biomacromolecules 20 (2019) 2058–2067.
[21] Y. Zha, T. Lin, Y. Li, X. Zhang, Z. Wang, Z. Li, Y. Ye, B. Wang, S. Zhang, J. Wang, Exosome-mimetics as an engineered gene-activated matrix induces in-situ vascularized osteogenesis, Biomaterials 247 (2020) 119985.
[22] J. Tan, M. Zhang, Z. Hai, C. Wu, J. Lin, W. Kuang, H. Tang, Y. Huang, X. Chen, G. Liang, Sustained release of two bioactive factors from supramolecular hydrogel promotes periodontal bone regeneration, ACS Nano 13 (2019) 5616–5622.
[23] L. Cui, J. Zhang, J. Zou, X. Yang, H. Guo, H. Tian, P. Zhang, Y. Wang, N. Zhang, X. Zhuang, Z. Li, J. Ding, X. Chen, Electroactive composite scaffold with locally expressed osteoinductive factor for synergistic bone repair upon electrical stimulation, Biomaterials 230 (2020) 119617.
[24] B.O. Okesola, S. Ni, B. Derkus, C.C. Galeano, A. Hasan, Y. Wu, J. Ramis, L. Buttery, J.I. Dawson, M. D'Este, R.O.C. Oreffo, D. Eglin, H. Sun, A. Mata, Growth-factor free multicomponent nanocomposite hydrogels that stimulate bone formation, Adv. Funct. Mater. 30 (2020) 1906205.
[25] B. Leader, Q.J. Baca, D.E. Golan, Protein therapeutics: a summary and pharmacological classification, Nat. Rev. Drug. Discov. 7 (2008) 21–39.
[26] Q. Wang, D. Shi, Y. Geng, Q. Huang, L. Xiang, Baicalin augments the differentiation of osteoblasts via enhancement of microRNA-217, Mol. Cell. Biochem. 463 (2020) 91–100.
[27] T. Li, P. Wang, W. Guo, X. Huang, X. Tian, G. Wu, B. Xu, F. Li, C. Yan, X.J. Liang, H. Lei, Natural berberine-based Chinese herb medicine assembled nanostructures with modified antibacterial application, ACS Nano 13 (2019) 6770–6781.
[28] J. Ming, L. Zhuoneng, Z. Guangxun, Protective role of flavonoid baicalin from Scutellaria baicalensis in periodontal disease pathogenesis: a literature review, Complement, Ther. Med. 38 (2018) 11–18.
[29] B. Dinda, S. Dinda, S. DasSharma, R. Banik, A. Chakraborty, M. Dinda, Therapeutic potentials of baicalin and its aglycone, baicalein against inflammatory disorders, Eur. J. Med. Chem. 131 (2017) 68–80.
[30] G. Cheng, C. Yin, H. Tu, S. Jiang, Q. Wang, X. Zhou, X. Xing, C. Xie, X. Shi, Y. Du, H. Deng, Z. Li, Controlled Co-delivery of growth factors through layer-by-layer assembly of core-shell nanofibers for improving bone regeneration, ACS Nano 13 (2019) 6372–6382.
[31] Z.G. Tang, N.P. Rhodes, J.A. Hunt, Control of the domain microstructures of PLGA and PCL binary systems: importance of morphology in controlled drug release, Chem. Eng. Res. Des. 85 (2007) 1044–1050.
[32] P. Liu, L. Sun, P. Liu, W. Yu, Q. Zhang, W. Zhang, J. Ma, P. Liu, J. Shen, Surface modification of porous PLGA scaffolds with plasma for preventing dimensional shrinkage and promoting scaffold-cell/tissue interactions, J. Mater. Chem. B. 6 (2018) 7605–7613.
[33] C. Ru, F. Wang, M. Pang, L. Sun, R. Chen, Y. Sun, Suspended, shrinkage-free, electrospun PLGA nanofibrous scaffold for skin tissue engineering, ACS Appl. Mater. Interfaces 7 (2015) 10872–10877.
[34] X. Feng, J. Li, X. Zhang, T. Liu, J. Ding, X. Chen, Electrospun polymer micro/nanofibers as pharmaceutical repositories for healthcare, J. Contr. Release 302 (2019) 19–41.

[35] H. Kim, L. Che, Y. Ha, W. Ryu, Mechanically-reinforced electrospun composite silk fibroin nanofibers containing hydroxyapatite nanoparticles, Mater. Sci. Eng., C 40 (2014) 324–335.
[36] H.M.A. Kolken, K. Lietaert, T. van der Sloten, B. Pouran, A. Meynen, G. Van Loock, H. Weinans, L. Scheys, A.A. Zadpoor, Mechanical performance of auxetic meta-biomaterials, J. Mech. Behav. Biomed. Mater. 104 (2020) 103658.
[37] G. Yang, X. Li, Y. He, J. Ma, G. Ni, S. Zhou, From nano to micro to macro: electrospun hierarchically structured polymeric fibers for biomedical applications, Prog. Polym. Sci. 81 (2018) 80–113.
[38] A. Li, J. Zhao, J. Liu, J. Shi, G. Rao, H. Wei, J. Gou, Effects of naringin and baicalin combination on the biological activity of human periodontal ligament cells, J. Pract. Stomatol. 27 (2011) 619–623.
[39] K.J. Rambhia, P.X. Ma, Controlled drug release for tissue engineering, J. Contr. Release 219 (2015) 119–128.
[40] X. Li, W. Luo, T.W. Ng, P.C. Leung, C. Zhang, K.C. Leung, L. Jin, Nanoparticle-encapsulated baicalein markedly modulates pro-inflammatory response in gingival epithelial cells, Nanoscale 9 (2017) 12897–12907.
[41] L.B. Jiang, D.H. Su, S.L. Ding, Q.C. Zhang, Z.F. Li, F.C. Chen, W. Ding, S.T. Zhang, J. Dong, Salt-assisted toughening of protein hydrogel with controlled degradation for bone regeneration, Adv. Funct. Mater. 29 (2019) 1901314.
[42] C. Shuai, W. Yang, P. Feng, S. Peng, H. Pan, Accelerated degradation of HAP/PLLA bone scaffold by PGA blending facilitates bioactivity and osteoconductivity, Bioact. Mater. 6 (2021) 490–502.
[43] D.J. Choi, S.M. Choi, H.Y. Kang, H.J. Min, R. Lee, M. Ikram, F. Subhan, S.W. Jin, Y. H. Jeong, J.Y. Kwak, S. Yoon, Bioactive fish collagen/polycaprolactone composite nanofibrous scaffolds fabricated by electrospinning for 3D cell culture, J. Biotechnol. 205 (2015) 47–58.
[44] Z. Pei, B. Wang, F. Zhang, Z. Niu, S. Shi, R.D. Cannon, L. Mei, Response of human periodontal ligament cells to baicalin, J. Periodontol. 85 (2014) 1283–1290.
[45] L.J. Chen, B.B. Hu, X.L. Shi, M.M. Ren, W.B. Yu, S.D. Cen, R.D. Hu, H. Deng, Baicalein enhances the osteogenic differentiation of human periodontal ligament cells by activating the Wnt/beta-catenin signaling pathway, Arch. Oral Biol. 78 (2017) 100–108.
[46] J. Gan, C. Liu, H. Li, S. Wang, Z. Wang, Z. Kang, Z. Huang, J. Zhang, C. Wang, D. Lv, L. Dong, Accelerated wound healing in diabetes by reprogramming the macrophages with particle-induced clustering of the mannose receptors, Biomaterials 219 (2019) 119340.
[47] A. Vishwakarma, N.S. Bhise, M.B. Evangelista, J. Rouwkema, M.R. Dokmeci, A. M. Ghaemmaghami, N.E. Vrana, A. Khademhosseini, Engineering immunomodulatory biomaterials to tune the inflammatory response, Trends Biotechnol. 34 (2016) 470–482.
[48] B.N. Brown, R. Londono, S. Tottey, L. Zhang, K.A. Kukla, M.T. Wolf, K.A. Daly, J. E. Reing, S.F. Badylak, Macrophage phenotype as a predictor of constructive remodeling following the implantation of biologically derived surgical mesh materials, Acta Biomater. 8 (2012) 978–987.
[49] P. Qiu, M. Li, K. Chen, B. Fang, P. Chen, Z. Tang, X. Lin, S. Fan, Periosteal matrix-derived hydrogel promotes bone repair through an early immune regulation coupled with enhanced angio- and osteogenesis, Biomaterials 227 (2020) 119552.
[50] M. Xu, X. Li, L. Song, Baicalin regulates macrophages polarization and alleviates myocardial ischaemia/reperfusion injury via inhibiting JAK/STAT pathway, Pharm. Biol. 58 (2020) 655–663.
[51] R.A. Bank, Limiting biomaterial fibrosis, Nat. Mater. 18 (2019) 781.
[52] W. Lee, S.K. Ku, J.S. Bae, Anti-inflammatory effects of baicalin, baicalein, and wogonin in vitro and in vivo, Inflammation 38 (2015) 110–125.
[53] C. Chen, C. Zhang, L. Cai, H. Xie, W. Hu, T. Wang, D. Lu, H. Chen, Baicalin suppresses IL-1 beta-induced expression of inflammatory cytokines via blocking NF-kappaB in human osteoarthritis chondrocytes and shows protective effect in mice osteoarthritis models, Int. Immunopharm. 52 (2017) 218–226.
[54] Q. Hu, L. Gao, B. Peng, X. Liu, Baicalin and baicalein attenuate renal fibrosis in vitro via inhibition of the TGF-beta 1 signaling pathway, Exp. Ther. Med. 14 (2017) 3074–3080.
[55] B. Tang, X. Wang, Y. Zhu, X. Li, S. Yao, Baicalin attenuates lipopolysaccharide-induced pro-inflammatory cytokine expression in murine macrophage cell line RAW264.7 through miR-124-STAT3 axis, Eur. J. Inflamm. 16 (2018) 1–10.
[56] H. Xing, X. Wang, G. Xiao, Z. Zhao, S. Zou, M. Li, J.J. Richardson, B.L. Tardy, L. Xie, S. Komasa, J. Okazaki, Q. Jiang, G. Yang, J. Guo, Hierarchical assembly of nanostructured coating for siRNA-based dual therapy of bone regeneration and revascularization, Biomaterials 235 (2020) 119784.
[57] Y. Kameo, Y. Miya, M. Hayashi, T. Nakashima, T. Adachi, In silico experiments of bone remodeling explore metabolic diseases and their drug treatment, Sci. Adv. 6 (2020), eaax0938.
[58] L. Lu, L. Rao, H. Jia, J. Chen, X. Lu, G. Yang, Q. Li, K.K.H. Lee, L. Yang, Baicalin positively regulates osteoclast function by activating MAPK/Mitf signalling, J. Cell Mol. Med. 21 (2017) 1361–1372.
[59] A.J. Guo, R.C. Choi, A.W. Cheung, V.P. Chen, S.L. Xu, T.T. Dong, J.J. Chen, K. W. Tsim, Baicalin, a flavone, induces the differentiation of cultured osteoblasts: an action via the Wnt/beta-catenin signaling pathway, J. Biol. Chem. 286 (2011) 27882–27893.
[60] L. Weng, S.K. Boda, H. Wang, M.J. Teusink, F.D. Shuler, J. Xie, Novel 3D hybrid nanofiber aerogels coupled with BMP-2 peptides for cranial bone regeneration, Adv. Healthcare. Mater. 7 (2018), e1701415.